Wlodek, M., Slastanova, A., Fox, L. J., Taylor, N., Bikondoa, O., Szwarzynski, M., Kolasińska-Sojka, M., Warszyński, P., & Briscoe, W. H. (2020). Structural evolution of supported lipid bilayers intercalated with quantum dots. *Journal of Colloid and Interface Science*, *562*, 409-417. https://doi.org/10.1016/j.jcis.2019.11.102

Journal Pre-proofs

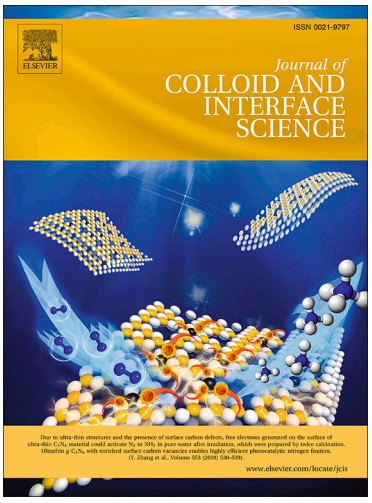

Structural evolution of supported lipid bilayers intercalated with quantum dots

Magdalena Wlodek, Anna Slastanova, Laura J. Fox, Nicholas Taylor, Oier Bikondoa, Michal Szuwarzynski, Marta Kolasinska-Sojka, Piotr Warszynski, Wuge H. Briscoe

PII: S0021-9797(19)31430-4
DOI: https://doi.org/10.1016/j.jcis.2019.11.102
Reference: YJCIS 25719

To appear in: *Journal of Colloid and Interface Science*

Received Date: 25 October 2019
Revised Date: 23 November 2019
Accepted Date: 25 November 2019

Please cite this article as: M. Wlodek, A. Slastanova, L.J. Fox, N. Taylor, O. Bikondoa, M. Szuwarzynski, M. Kolasinska-Sojka, P. Warszynski, W.H. Briscoe, Structural evolution of supported lipid bilayers intercalated with quantum dots, *Journal of Colloid and Interface Science* (2019), doi: https://doi.org/10.1016/j.jcis.2019.11.102

Structural evolution of supported lipid bilayers intercalated with quantum dots

Magdalena Wlodek[a*], Anna Slastanova[b], Laura J. Fox[b], Nicholas Taylor[b], Oier Bikondoa[c], Michal Szuwarzynski[d], Marta Kolasinska-Sojka[a], Piotr Warszynski[a] and Wuge H. Briscoe[b*]

[a]Jerzy Haber Institute of Catalysis and Surface Chemistry, Polish Academy of Sciences, Niezapominajek 8, PL-30239 Krakow, Poland

[b]School of Chemistry, University of Bristol, Cantock's Close, Bristol BS8 1TS, United Kingdom

[c]XMaS, The UK-CRG Beamline, The European Synchrotron (ESRF), 71 Avenue des Martyrs, 38043 Grenoble, France. Department of Physics, University of Warwick, Gibbet Hill Road, Coventry CV4 7AL, United Kingdom

[d]AGH University of Science and Technology, Academic Centre for Materials and Nanotechnology, al. A. Mickiewicza 30, PL-30059 Krakow, Poland

*Corresponding authors. MW: e-mail: ncwlodek@cyf-kr.edu.pl; WHB: Tel. +44 117332856, email: wuge.briscoe@bristol.ac.uk

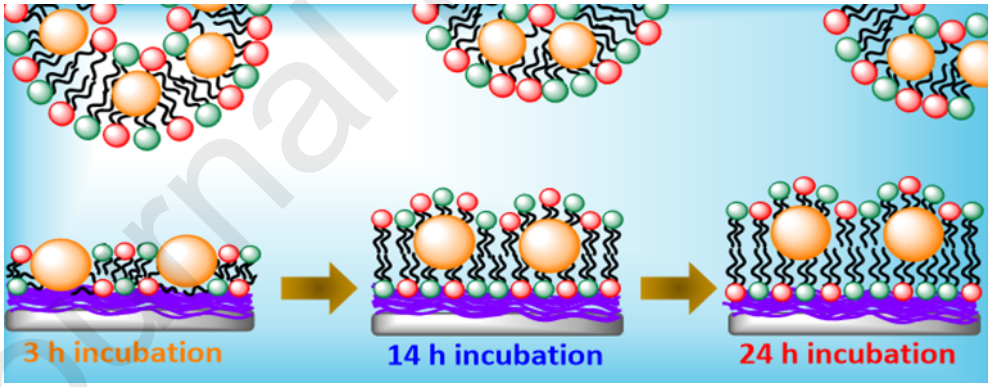

Abstract

Hypothesis: Supported lipid bilayers (SLBs) embedded with hydrophobic quantum dots (QDs) undergo temporal structural rearrangement.

***Experiments*:** Synchrotron X-ray reflectivity (XRR) was applied to monitor the temporal structural changes over a period of 24 h of mixed SLBs of 1-palmitoyl-2-oleoyl-sn-glycero-3-phosphocholine (POPC) / 1-palmitoyl-2-oleoyl-sn-glycero-3-phospho-ethanolamine (POPE) intercalated with 4.9 nm hydrophobic cadmium sulphide quantum dots (CdS QDs). The QD-embedded SLBs (QD-SLBs) were formed *via* rupture of the mixed liposomes on a positively

charged polyethylene imine (PEI) monolayer. Atomic force microscopy (AFM) imaging provided complementary characterization of the bilayer morphology.

***Findings*:** Our results show time-dependent perturbations in the SLB structure due to the interaction upon QD incorporation. Compared to the SLB without QDs, at 3 h incubation time, there was a measurable decrease in the bilayer thickness and a concurrent increase in the scattering length density (SLD) of the QD-SLB. The QD-SLB then became progressively thicker with increasing incubation time, which – along with the fitted SLD profile – was attributed to the structural rearrangement due to the QDs being expelled from the inner leaflet to the outer leaflet of the bilayer. Our results give unprecedented mechanistic insights into the structural evolution of QD-SLBs on a polymer cushion, important to their potential biomedical and biosensing applications.

Keywords: Supported lipid bilayers; X-ray reflectivity (XRR); Nanoparticle-membrane interactions; Membranes intercalated with quantum dots; Bilayer structure

INTRODUCTION

Supported lipid bilayers (SLBs) are widely used as model cell membranes[1] and also have potential applications in diagnostic devices and biomimetics.[2,3] The SLB structure and functionality is underpinned by the fluidity and mobility of the lipid molecules and their interactions with the substrate.[4,5] Several methods have been developed for SLB formation including vesicle fusion,[6–8] evaporation induced assembly,[9] spin-coating,[10] co-adsorption from mixed lipid-surfactant micellar solutions,[11] and Langmuir-Blodgett/Schaefer deposition.[12–14] Of these, spontaneous fusion of small unilamellar lipid vesicles (SUVs) on hydrophilic solid supports, pioneered by McConnell *et al*.,[15] represents a facile route for formation of SLBs of different lipid compositions. Another advantage of this method is the capacity and ease to incorporate functionalized additives (*e.g.* amphiphilic proteins[16], metal nanoparticles[17] or quantum dots[18,19]) to the membrane.

The mechanism for SLB formation *via* adsorption and fusion of SUVs has been proposed to follow either a one-step or two-step process. In the one-step process, upon initial SUV attachment to the substrate surface, if the adhesion is strong enough or the vesicles are in a stressed state, they may deform and the consequent intra-bilayer stress may lead to vesicle rupture, resulting in the formation of small fragmented SLB patches on the surface.[20] A two-step SLB formation process takes place in the case of weak vesicle adhesion, where vesicles would require additional stress from neighbouring vesicles to cause rupture, which is reached at a critical surface vesicle coverage, θ_c (or critical surface density). After initial vesicle rupture,

they can subsequently fuse through hydrophobic interactions between the unfavourable edges of the bilayer patches, as well through the highly curved regions of the stressed vesicles. This process continues until the bilayer is complete, and then excess lipids and water may be ejected back into solution. This two-step process is driven by the membrane tension of the adsorbed vesicles, vesicle-vesicle and vesicle-surface interactions.[20] The strength of these interactions can be tuned by experimental conditions, including vesicle size[21] and concentration,[22] temperature,[23] pH,[22] ionic strength[3] of the solution, addition of specific ions,[24] and substrate surface chemistry.[25–27] Generally, four different pathways for vesicle rupture and unfolding of the vesicle membrane on the surface have been suggested.[28] The vesicles can rupture either the outer (*pathway 1*) or the inner leaflet (*pathway 2*), or their membrane can undergo division into fragments (*pathways 3* and *4*).[28] In *pathway 3*, the upper membrane fragments slide down and adsorb on the surface next to the bottom bilayer fragments in the original contact; whereas in *pathway 4*, the upper membrane fragments desorb to the bulk solution.

Nanoparticles (NPs) can be incorporated into SLBs to form NP-SLB hybrids, which are promising candidates for bioanalytical applications, *e.g.* tracking of vesicle fusion on surfaces *via* fluorescence visualization of the NPs in the resulting lipid bilayers.[29,30] Moreover, QD-SLBs hybrids represent a promising platform in biotechnology, for instance for novel devices with features of flexible structures such as single-electron transistors, plasmonic devices and biotransitors.[17,31] In addition, studying the structure of QD-SLBs hybrids is also relevant to understanding the interactions between functional NPs and model cell membranes. Considering its crucial importance to the design and use of nanomaterials in biomedical applications, there is an urgent need for a better fundamental understanding of NPs' roles in the lipid reorganization and the membrane morphology of NP-SLBs.[32] Several studies have shown that NPs can strongly interact with cell membranes, either adsorbing onto the membrane surface or penetrating the membrane, resulting in structural disruptions.[33] It has been shown that cationic NPs interact more strongly with zwitterionic lipid bilayers compared with uncharged or anionic nanoparticles. Moreover, it has been observed that binding of quantum dots (QDs) on lipid bilayers depended on the molecular packing in the bilayers.[34] AFM imaging by Mensch *et al.* showed that the introduction of QDs functionalized with the cationic polymer poly(diallyldimethylammonium chloride) (PDDA) to phase-segregated bilayers led to shrinking and eventual diminishment of the liquid-ordered L_o phase regions.[35] Further, it has been also shown that both membrane bending modulus and the NP size affect the wrapping of hydrophilic NPs and, therefore, their ability to interact with the membrane.[36,37] Moreover,

Mendozza *et al.*[38] demonstrated that inorganic gold (Au) and Superparamagnetic Iron Oxide (SPIO) NPs modified the phase behaviour and viscoelastic properties of non-lamellar Phytantriol (Phyt) lipid mesophases. The NP surface chemistry and size modulated the local perturbations of the lipid assemblies and affected the phase behaviour, while the chemical nature of NPs affected the mesophase viscoelastic response to mechanical perturbation and subsequent relaxation.

Despite numerous studies, there is a gap in our knowledge regarding how NPs can affect the SLB formation process. Little is known of the NP localization and distribution within the lipid assemblies upon vesicle fusion and SLB formation; or how the NP presence would change the SLB structure and physicochemical properties. Such an understanding is important for optimisation of NPs-SLBs-hybrid structures for future applications.

NP-induced SLB structural rearrangement at the buried solid-liquid interface can be difficult to observe. In this context, X-ray reflectivity (XRR) can provide structural insights into NP-SLB formation, as the high flux of synchrotron X-rays can facilitate time-resolved measurements and shed light on the temporal structural evolution of NP-SLBs during their formation. For this reason, XRR is the main method employed in the current study. We should comment that, with the development of high flux modern neutron sources, neutron reflectivity (NR) will also be suitable for structural investigations of buried interfaces with good temporal resolution, which also offers the advantage of contrast variation *via* selective deuteration.

The main aim of this study was to investigate structural changes of negatively charged POPC/POPE supported lipid bilayers intercalated with quantum dots on a poly(ethyleneimine) (PEI) monolayer as a function of incubation time, using *in situ* synchrotron XRR, with the resulting morphology imaged by atomic force microscopy (AFM). POPC and POPE are common lipids found in bacterial and eukaryote membranes,[39] and their mixed bilayers have been widely studied as model membranes. Hydrogen bonding formation among PE lipids and between the PE headgroup and the solid support could also promote vesicle fusion and SLB formation.[40,41] Whilst symmetric bilayers consisting of zwitterionic phospholipids have been widely studied, relatively less attention has been paid to such negatively charged lipid bilayers. Their charges would lead to different interactions with NPs compared to the zwitterionic lipids. Moreover, this study is also motivated by our recent report on incorporation of hydrophobic cadmium sulphide quantum dots (CdS QDs) with size 2.7 – 5.4 nm into mixed POPC/POPE SLBs *via* liposome fusion.[18] The QDs were found embedded in the hydrophobic regions of the SLBs, retaining the QD fluorescence properties. Our findings opened up a new route for preparation of fluorescent QD-endowed SLBs *via* liposome fusion

for potential bioanalytic applications, for which it is critically important to understand the structure and formation kinetics of QD-endowed SLBs.[18] The quartz crystal microbalance with dissipation monitoring (QCM-D) data in the study also indicated that the QD-endowed liposomes ruptured at a lower critical surface coverage θ_c compared to the pure liposomes, suggesting that the presence of the QDs would have affected the SLB formation kinetics, an effect investigated in the present study.

Here, we have used 4.9 nm CdS QDs, for which a high effective loading efficiency into the alkyl tails region of POPC/POPE liposomes was achieved as estimated by fluorimetric experiments. The SLB was formed on a PEI film, which has been previously shown[27,42,43] as an effective anchor for adsorption of nanoobjects such as polyelectrolytes, nanoparticles, or liposomes. In our study, the PEI monolayer preparation used the same procedure as that in those previous studies, and the detailed characterization of such PEI monolayer has also been reported by Adamczyk *et al*.[44] Our XRR results reveal the temporal structural evolution of QD-embedded SLBs on the PEI cushion during a period of 24 h upon initial surface-fusion, due to reorganization of lipid molecules and QD rearrangement. Our findings are relevant to the fundamental understanding of interactions between NPs and lipid membranes, particularly how NPs might affect the SLB formation process, and provide useful information on the structure of the nanoparticle-embedded SLBs, important to their applications and cytotoxicity.

MATERIALS AND METHODS

Materials

The branched poly(ethyleneimine) (PEI, M_w 750 kDa) was obtained from Sigma-Aldrich (Germany). 1-palmitoyl-2-oleoyl-*sn*-glycero-3-phosphocholine (POPC) and 1-palmitoyl-2-oleoyl-*sn*-glycero-3-phosphoethanolamine (POPE) lipids were purchased from Avanti Polar Lipids. Cadmium sulphide quantum dots (CdS QDs) surface-stabilized with oleic acid coating (5.0 mg/mL in toluene) were purchased from Sigma-Aldrich, which specified a typical nanocrystal size of 4.9 nm with the corresponding fluorescence emission maximum wavelength at 440 nm. NaCl (99.5 %) used for PEI solutions preparation was obtained from Fluka. H_2SO_4 (96 %) and H_2O_2 (32 %) used for silicon wafers cleaning procedure from Sigma-Aldrich. Phosphate buffer (PBS) was made of NaCl, Na_2HPO_4 and NaH_2PO_4, and its pH was regulated to 9.5 by the addition of an appropriate amount of NaOH. Ultrapure, Milli-Q water (resistivity > 18 MΩ cm and total organic content < 5 ppb) was used for all solution preparation. For the substrate, silicon wafers (On semiconductor, Czech Republic) with orientation <100> were used. They were cleaned by submerging for 30 min in a piranha solution, which is a mixture of

equivalent volumes of concentrated sulfuric acid and perhydrol (*Precaution! This solution is a very strong oxidizing agent and should be handled carefully*). This was followed by rinsing with Milli-Q water and then submerging for 30 min in Milli-Q water at ~70^{o} C. The silicon wafers were pre-coated with PEI by dipping them into the polymer solution for 15 min, rinsing three times for 1 min each in Milli-Q water and dried with nitrogen. To prepare SLBs without or with embedded CdS-QDs, the vesicle fusion method was used.[18]

Preparation of liposomes with embedded quantum dots: Liposomes with QDs (QD-Ls) were prepared using the thin film hydration method. Typically, 150 µL of a 4.9 nm CdS suspension in toluene (5.0 mg/mL) was mixed with 5.0 mg of POPC and 5.0 mg of POPE phospholipids in 850 µL of chloroform. Assuming a QD density of 4.8 g/cm^3, this corresponded to a QD-lipid number ratio of $\nu = 3.1\times10^{-4}$ or a volume ratio of $\phi = 1.4\times10^{-2}$. This yielded a lipid-QD mixture suspension with a QD concentration of 0.75 mg/mL. Then, the solvent was evaporated under vacuum (50 mbar) for 24 hours approximately. The dried QD-L film was hydrated in 2.0 mL phosphate buffer with an ionic strength 0.2 M at pH = 9.5. The obtained multilamellar vesicles (MLVs) were further ultrasonicated with a sonicator bath for 20 min at room temperature. The resulting suspension was extruded in two series, each of 15 times through polycarbonate membranes with nominally 200 nm (first series) and 100 nm (second series) pores using a mini-extruder (Avanti Polar Lipids), and then diluted to the final concentration of 0.1 mg/mL SUV suspension.

Experimental Techniques

Synchrotron X-ray reflectivity (XRR) measurements

The XRR measurements were performed at beamline BM28 (XMaS) at the European Synchrotron Radiation Facility (ESRF), Grenoble, France. All the measurements were carried out within a closed liquid cell at room temperature which allowed *in situ* solution exchange.[45] The SLBs were formed by incubating PEI-coated silicon/silica substrates in SUV and QD-SUV dispersions, respectively. The measurements were carried out at 3 h, 14 h and 24 h incubation. The XRR measurements were performed on the same substrate (POPC/POPE SLBs with or without QDs on PEI monolayer coated silica) at different incubation times. The XRR curves collected from three different synchrotron experiments were reproducible. The BM28 monochromator was tuned to select an X-ray beam energy of 14.0 keV with a corresponding wavelength $\lambda = 0.886$ Å. The incident beam size, defined by slits, was 100 µm (vertical) and 240 µm (horizontal) at its full width at half maximum (FWHM). In each measurement, a monochromatic X-ray beam was incident upon the sample surface at some known grazing angle

θ_i (varying from 0.06° to ~ 2.5°), corresponding to a range (0.014-0.6 Å^{-1}) of the momentum transfer vector Q (=4π sin $(\frac{2\theta_i}{2})/\lambda$) normal to the surface. The specularly reflected intensity was detected at each angle $\theta_r = \theta_i$ using an avalanche photodiode detector (APD). The measured reflectivity curves were analysed using Motofit[46] in IGOR Pro (WaveMetrics, Portland, USA). The obtained reflectivity curves were optimised by the least χ^2 method using the Abeles matrix formalism as implemented in Motofit, in which the SLBs were treated as slabs of different scattering densities. To fit the experimental data of the pure SLB, different models have been developed. In the models, the structure of the bilayer on the substrate has been divided to four-, six- or seven-slabs. A summary of the structural parameters obtained from the analysis of XRR data are included in the **Supporting Material (SM).** In our study, the fit shown below is based on a six-slab model, which best described the XRR data of both the SLBs and the QD-SLBs, with the slabs labelled $n = 1 – 6$ in **Figure 1** consisting of: **(1)** the outer headgroup layer to the PBS buffer superphase (*o*-H), **(2)** the outer hydrocarbon tail layer (*o*-T), **(3)** the inner hydrocarbon tail layer (*i*-T), **(4)** the inner headgroup layer (*i*-H), **(5)** poly(ethyleneimine) layer (PEI), and **(6)** silicon oxide layer (SiO_2). The obtained fitting parameters such as the thickness t_n, scattering length density (SLD) ρ_n and interfacial roughness σ_n facilitated comparisons of the structural changes of the lipid bilayers as a function of the incubation time.

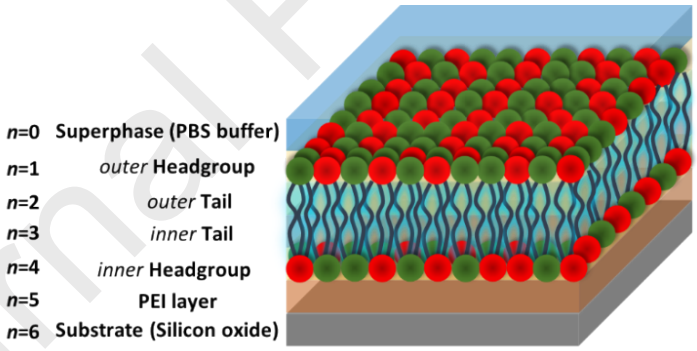

Figure 1. Schematic representation of the six-slab model used for fitting experimental data.

Atomic force microscopy (AFM)

AFM images were obtained with a Dimension Icon atomic force microscope (Bruker, Santa Barbara, CA) working in the fluid in the Peak Force Tapping™ (PFT) mode. Standard silicon cantilevers for PFT in fluids (Bruker) with a nominal spring constant of 0.7 N m^{-1} and a tip radius <10 nm were used for these measurements. Collected data was processed using Nanoscope Analysis 1.9 (Bruker). The plane fit (order 1) and flatten (order 0) corrections were applied to level all the AFM images. Areas with lipid patches were excluded from the correction

process using threshold option. The SLBs and QD-SLBs used the same preparation procedure as those in the XRR measurements.

RESULTS AND DISCUSSION

Figure 2 (**A**)-(**C**) shows the XRR curves of POPC/POPE lipid bilayers in the absence (lower orange curves) and in the presence of (upper red curves; offset on the vertical scale for clarity) 4.9 nm CdS QDs at 3 h, 14 h, and 24 h incubation time, respectively. The insets show the corresponding scattering length density (SLD) profiles obtained from data fitting, with the zero distance defined at the inner headgroup – PEI interface.

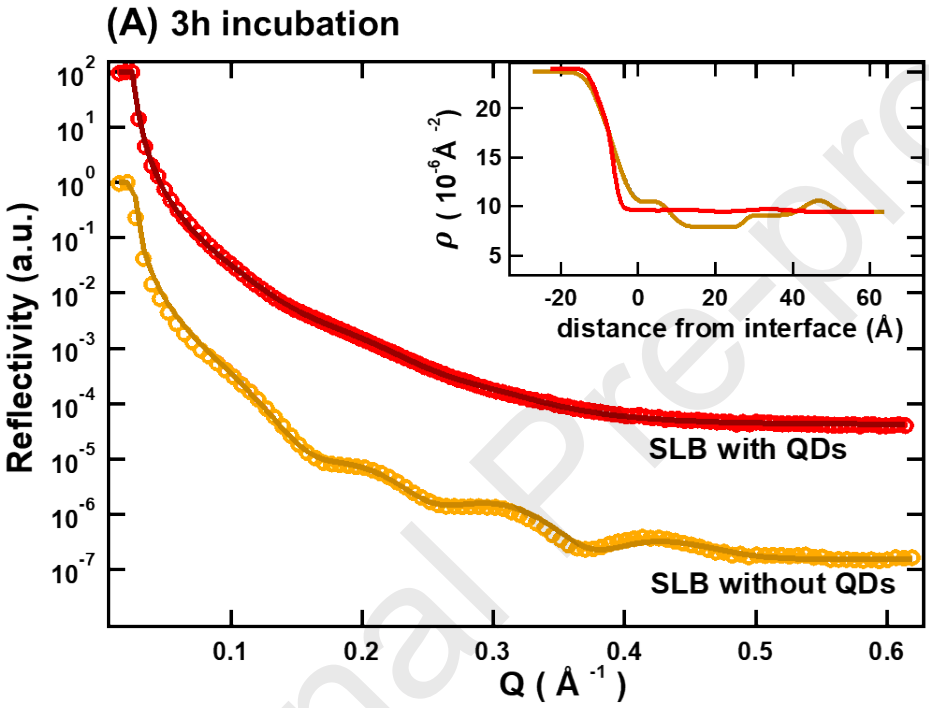

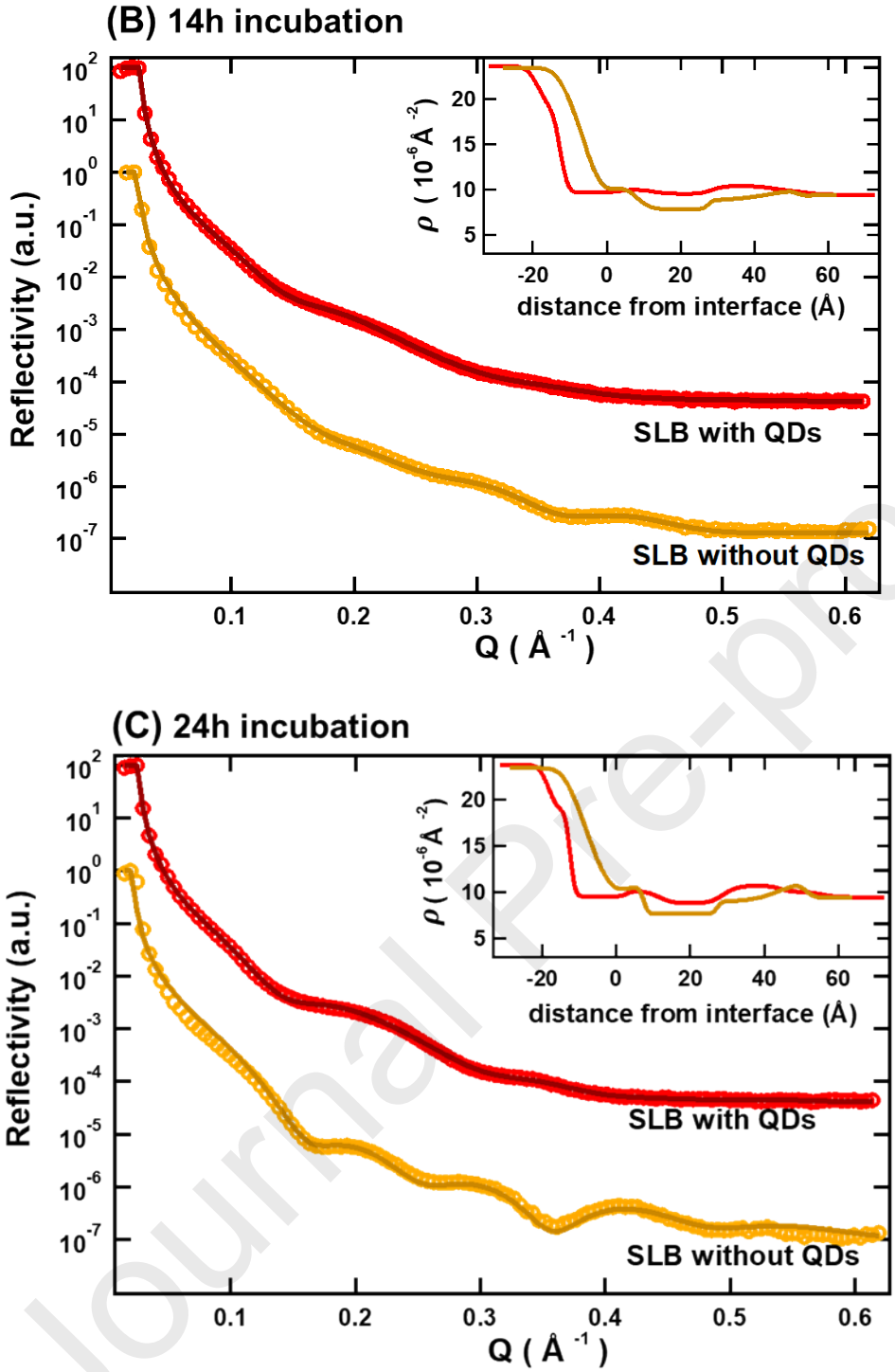

Figure 2. X-ray reflectivity (XRR) curves from POPC/POPE SLB without (lower curve) and with (upper curve) QDs formed on PEI monolayer after 3 h (A), 14 h (B) and 24 h (C) incubation. The symbols are experimental data points and the solid lines the best fit to the respective data. The corresponding scattering length density (SLD) profiles extracted from the fits are shown in inset.

Overall, the XRR curves were qualitatively different for the SLBs with and without the QDs at all the incubation times, and how the XRR curve evolved with the incubation time was also different. In the absence of CdS QDs, the Kiessig fringes (*i.e.* intensity oscillations) in the XRR profile were already pronounced at 3 h incubation time (the lower orange curve in **Figure 2**

(A)) and were retained at longer incubation time (**Figure 2 (B), (C)**). Such POPC/POPE mixed bilayer formation has also been previously confirmed by QCM-D measurements.[18,27]

We first trialled fitting the SLB XRR curves with a four-slab model, with the fitting parameters listed in **Table S2** in the **SM**, which describes an *asymmetric* bilayer with a total thickness t ~ 48.2 Å atop a PEI monolayer of 11.2 Å in thickness. To gain more structural insights, the XRR curves were then fitted with six- and seven-slab models. In these models, the bilayer structure has been divided to four layers of different SLDs: an inner headgroup layer (*i*-H), an inner tail layer (*i*-T), an outer headgroup layer (*o*-H), an outer tail layer (*o*-T), so that the inner (proximal to the substrate) and the outer (distal to the substrate) leaflets could be considered separately. It has been previously reported that they exhibit different thermodynamic behaviours due to the lipid-substrate interaction.[47]

In the case of the seven-slab model, an additional layer of lipid patches on top of the asymmetric membrane has been included, with the results collated in **SM**. This is in agreement with the neutron reflectivity (NR) study by Lind *et al*.,[8] who found lipid patches on top of the adsorbed lipid bilayer, with a low coverage and thickness of ~14.0 Å. The overriding structural feature revealed by the six- and seven-layer models is an asymmetric mixed bilayer of POPC/POPE. It should be noted that in the case of the QD-SLBs, not all data could be fitted with the four- and seven-slab model. The fitting parameters of the QD-SLB XRR curves have been listed in **SM**. The $\boldsymbol{\chi^2}$ values for the fitting parameters from different models are listed in **Table S6** in the **SM**, only indicative of the goodness of the fit. These values are similarly small. However, from **Figure S2** in **SM**, it is clear that the fits using the four-slab and seven-slab models were not as good as using the six-slab model **Figure 4**.

The discussion below is based on a six-slab model which consistently describes the XRR data for both the SLBs and QD-SLBs, a model also used in our previous study,[18] allowing a direct comparison of the bilayer structures in the absence and presence of the QDs. The fitted structural parameters are listed in **Table 1** and the fitted SLD profiles plotted in the insets to the **Figure 2** (orange SLD profiles). The fitted total thickness of the **POPC/POPE SLB** was t = 48.3 Å, 49.4 Å and 49.9 Å at 3 h, 14 h and 24 h incubation time, respectively, increasing slightly with the incubation time. The thickness is in agreement with the literature values from molecular dynamic simulations[48], XRR[49], and NR[50] measurements. As shown in the SLD profiles and illustrated in Figure **2 (A)** and **(B)**, the outer hydrocarbon tails thickness, $t_{o\text{-}T}$, increasing from 15.0 Å at 3 h to 16.9 Å at 24 h (*i.e.* an increment of Δt_T = 1.9 Å), while the inner hydrocarbon tail thickness remained largely constant at $t_{i\text{-}T}$ ~ 19.9 Å. Furthermore, the higher SLD of the outer hydrocarbon chains of POPC/POPE can be attributed to incomplete

coverage (*i.e.* patchy coverage, so that the SLD included the contribution from the higher SLD value of water), whilst the SLD of the inner hydrocarbon tails indicating densely-packed and fully-stretch lipid tails. This is consistent with an *asymmetric* bilayer. The structural differences between the two bilayer leaflets could arise from the asymmetrical distribution of POPC and POPE phospholipids in the two bilayer leaflets, and could also be related to the different molecular organization/packing in the two leaflets, which would lead to different chain mobility.

It is known, that the PE headgroup can form hydrogen bonds with water, affecting the structure of water hydrogen bonding network, and water molecules may also bridge neighbouring PE lipids.[51] Such intra-bilayer hydrogen bonds could direct the organization of lipid domains. As reported in [52], the presence of PE induced the formation of domains of either liquid-ordered or gel phases in mixed 1,2-dilauroyl-sn-glycero3-phosphoethanolamine (DLPE) / 1,2-dilauroyl-sn-glycero-3- phosphocholine (DLPC) membranes. Moreover, from atomic-scale molecular dynamic simulations of a supported asymmetric lipid membrane composed of a POPE inner leaflet and a POPC outer leaflet, it was found that the POPE lipids were more densely packed than the POPC lipids.[53] Furthermore, Ericher *et al.*[54] demonstrated that it was energetically more favourable for POPE to be located in the inner leaflet of asymmetric mixed POPC/POPE vesicles. The fitted inner headgroup thickness in **Table 1**, $t_{i\text{-H}} \sim 5.5$ Å, was smaller as compared with the outer headgroup thickness, $t_{o\text{-H}} = 7.9$ Å, which suggests that the inner leaflet of POPC/POPE SLBs was possibly enriched with the PE lipids with a smaller headgroup, thus not inconsistent with the previous findings. The PE enrichment in the inner leaflet could also be encouraged by greater attraction between the negatively charged PE headgroups and the positively charged PEI cushion.

Table 1. Fitted bilayer structural parameters from the six-layer model for the POPC/POPE SLB without QDs on a PEI monolayer at 3 h, 14 h and 24 h incubation time. t_n, ρ_n and σ_n denote the thickness, scattering length density (SLD) and roughness of the n^{th} slab respectively. Errors for the parameters determined using minimization of χ^2 are < 0.8% from the fitting.

n^{th} slab	slab	*3h incubation*			*14h incubation*			*24h incubation*		
		t_n (Å)	ρ_n (10^{-6} Å^{-2})	σ_n (Å)	t_n (Å)	ρ_n (10^{-6} Å^{-2})	σ_n (Å)	t_n (Å)	ρ_n (10^{-6} Å^{-2})	σ_n (Å)
1	***o*-H**	7.5	11.1	2.8	8.4	10.1	1.1	7.9	10.9	1.1
2	***o*-T**	15.0	9.0	3.0	15.8	8.8	7.6	16.9	9.0	5.9
3	***i*-T**	20.0	7.8	0.5	19.7	7.8	0.5	19.9	7.8	1.4
4	***i*-H**	5.8	11.1	2.7	5.5	10.1	3.0	5.2	10.0	2.2
	Total Bilayer	**48.3**			**49.4**			**49.9**		

5	**PEI**	7.0	9.6	3.2	7.6	9.6	2.8	8.0	9.7	3.1
6	**SiO_2**	5.8	18.7	3.3	5.8	18.7	3.2	5.8	18.7	3.3

For the SLBs containing QDs (QD-SLBs), the XRR profiles appeared qualitatively different compared to the pure SLB XRR curves. The differences are also evident from the fitted SLD profiles in the insets in **Figure 2** (red curves), and the incorporation of QDs in the bilayers is evident from the fitted SLD which is higher than that of the pure SLB, attributed to the higher SLD of CdS QDs ($\rho = 36.1\times10^{-6}$ Å^{-2}). At 3 h incubation, the Kiessig fringes were very mild compared to the pure SLB, with a fitted bilayer thickness of t = 44.2 Å. With the increasing incubation time, the XRR profiles exhibited more pronounced Kiessig fringes, indicating a different structure of the QD-SLBs that evolved with time. The fitted bilayer thickness was t = 49.1 Å and 52.9 Å at 14 h and 24 h incubation time, respectively. The fitting parameters of QD-SLBs XRR curves are summarized in **Table 2.** It is worth noting that the fitted SLD and the thickness of the QD-SLB inner and outer leaflet also indicate an *asymmetric* bilayer structure, as with the case of the SLB without the QDs.

The total QD-SLB thickness was the smallest at 3 h incubation, which could be attributed to tilted or interdigitated lipid chains. The interactions upon QD incorporation into the hydrophobic region of the bilayer can have a direct effect on the chain configuration. It could, in turn, lead to strong perturbations in the self-assembled bilayer structure resulting in thinner lipid bilayers as the lipid tails tilt to preferentially interact with the hydrophobic QDs, forming a thinner bilayer. As schematically shown in **Figure 3 (C)**, the incorporation of the QDs induced changes in the local curvature of the bilayer leaflets, which could lead to tilt deformations. May *et al.*[55] showed that the lipid tilt modulus consisted of two major contributions: elastic component resulting from the tilt-induced stretching of the hydrocarbon chains and an entropic contribution from the constraints imposed by chain tilting on the fluctuations of chain orientations. In our case, the entropic contribution due to QD-induced chain re-orientation and inhomogeneous lateral distributions of the lipids could contribute to the chain tilt modulus.

Consequently, the hydrophobic QDs would cause structural disorder evident from a pronounced interfacial roughness at the water-bilayer interface (σ = 5.5 Å). This interpretation is consistent with the study by Bhattacharya *et al.*[56] who observed that the DPPC bilayer thickness decreased as a result of the addition of an ionic liquid. The QD diameter 49.0 Å is greater than the total bilayer thickness (t = 44.2 Å), suggesting that the QDs were partially embedded in the lipid bilayer or partially protruding from bilayer surface. This could also

contribute to the relatively high roughness value of σ = 5.5 Å, 4.9 Å and 2.2 Å observed for the outer headgroup layer and both hydrocarbon chains at 3 h incubation, respectively.

Moreover, evident from the fitting parameters in **Table 2**, as schematically shown in **Figure 3 (A)** and **(C)**, the outer and inner leaflets of the QD-SLBs exhibited noticeably different structures, which also changed with the incubation time. Their thickness t differed, with the total inner leaflet t_i (3 h) = t_{ih}+t_{it} = 19.8 Å, t_i (14 h) = 25.1 Å, and t_i (24 h) = 26.2 Å; for the outer leaflet, t_o (3 h) = 24.4 Å, t_o (14 h) = 24.0 Å, and t_o (24 h) = 26.7 Å. After 24 h incubation, the outer leaflet became thicker, as the headgroup expanded to $t_{o\text{-H}}$ = 11.0 Å, larger than that at 3 h incubation. This could have two explanations. First, the QD rearrangement could lead to a slight tilt of the lipid headgroups; alternatively, the thicker outer layer could be due to an overall more fluid and mobile layer, leading to more water molecules associated with the lipid headgroups.

Table 2. Fitted bilayer structural parameters from the six-layer model of QD-SLB on a PEI monolayer at 3 h, 14 h and 24 h incubation time. t_n, ρ_n and σ_n denote the thickness, scattering length density (SLD) and roughness of the n^{th} slab respectively. Errors for the parameters determined using minimization of χ^2 are < 0.05% from the fitting.

n^{th} slab	slab	*3h incubation*			*14h incubation*			*24h incubation*		
		t_n (Å)	ρ_n (10^{-6} Å^{-2})	σ_n (Å)	t_n (Å)	ρ_n (10^{-6} Å^{-2})	σ_n (Å)	t_n (Å)	ρ_n (10^{-6} Å^{-2})	σ_n (Å)
1	***o*-H**	8.4	10.1	5.5	8.6	10.1	4.8	11.0	10.0	2.9
2	***o*-T**	16.0	9.7	4.9	15.4	10.4	2.8	15.7	10.6	2.3
3	***i*-T**	11.4	9.9	2.2	16.0	9.5	2.4	17.3	8.7	2.9
4	***i*-H**	8.4	10.0	4.9	9.1	10.0	3.3	8.9	10.1	2.9
	Total Bilayer	**44.2**			**49.1**			**52.9**		
5	**PEI**	12.5	9.7	2.8	15.9	9.7	2.9	15.2	9.5	1.3
6	**SiO_2**	5.8	18.7	1.7	5.8	18.7	1.6	5.8	18.7	1.1

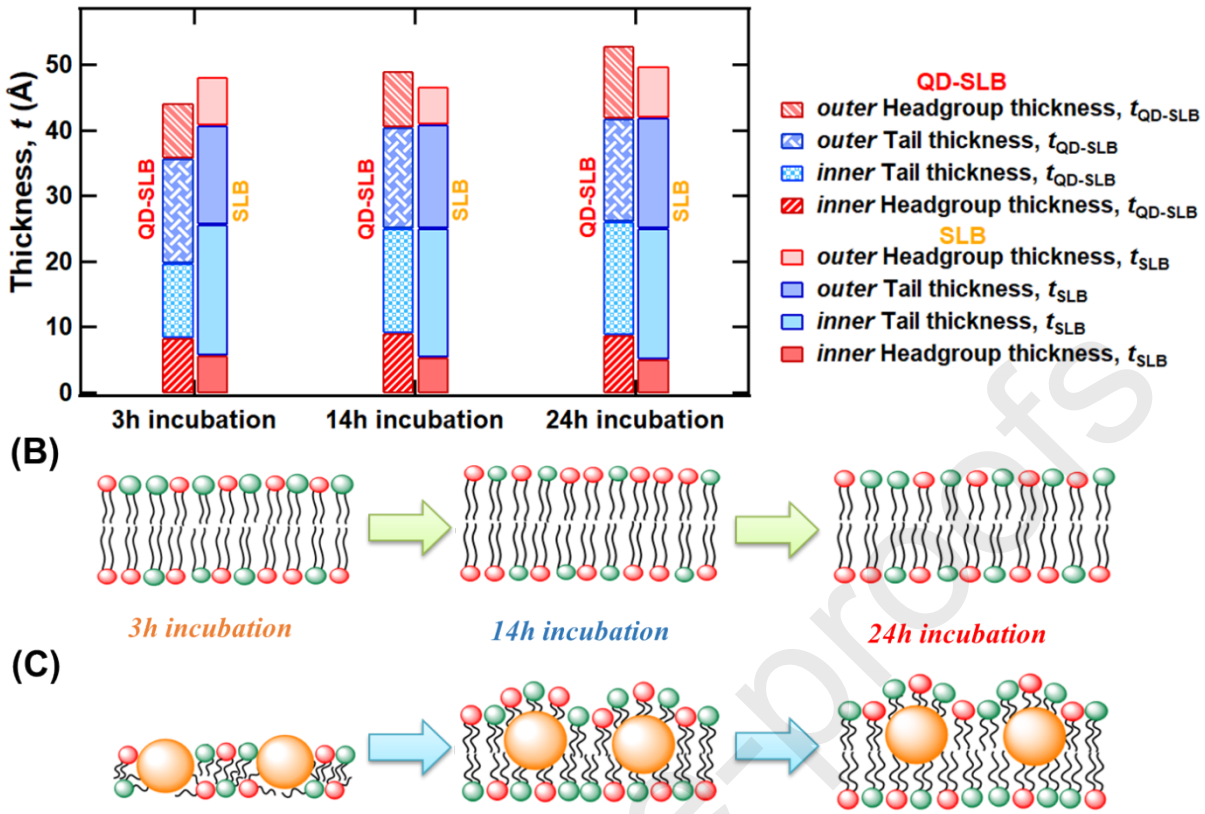

Figure 3. The thicknesses *t* of the proximal (inner) and the distal (outer) leaflets in the QD-SLB and SLB are compared in (A). The schematic representation of the mixed POPC/POPE SLB (B) and QD-SLB (C) at different incubation times suggested by their fitted SLD profiles of the XRR data.

In addition to such a comparison between the bilayer structures in the absence and presence of the QDs, time-resolved XRR measurements also show that the QD-SLB structure evolved with the incubation time, evident from the changes in the XRR Kiessig fringes. The XRR curves in **Figure 4 (A)** are plotted as RQ^4 vs. Q to more clearly show the reflectivity intensity oscillations at higher Q.[57] Qualitatively, the Kiessig fringes became more pronounced with the incubation time; and the minimum at $Q_z \approx 0.15$ Å^{-1} became deeper until it reached a minimum at 24 h incubation, consistent with bilayer thickening with time. The fitted bilayer thickness increased from $t = 44.2$ Å at 3 h to $t = 52.9$ Å at 24 h. It has been previously reported in several molecular dynamics simulation and experimental studies[58–60] that hydrophobic NPs, when adsorbing on the membrane, could cause lipid re-organization and bilayer thinning. This is consistent with our observations at 3 h incubation, where the bilayer thickness of the QD-SLB ($t = 44.2$ Å) was smaller than that of SLB without QDs ($t = 48.3$ Å), a thinning of $\Delta t = 4.1$ Å. With the increasing incubation time to 14 h and 24 h, the QD-SLB thickness became comparable to that of SLD, and then slightly thicker, indicative the structural rearrangement in the bilayer.

The marked change in the structure of the QD-SLBs bilayer is also consistent with the fitted SLD profiles of the QD-SLBs, which show a corresponding change with the incubation time. The SLD profiles gradually increased in the outer hydrocarbon tails (*o*-T), from ρ_{o-T} = 9.7 × 10^{-6} Å^{-2} at 3 h to value of ρ_{o-T} = 10.6 × 10^{-6} Å^{-2} at 24 h, and concurrently decreased in the inner hydrocarbon tails (*i*-T) from ρ_{i-T} = 9.9 × 10^{-6} Å^{-2} to ρ_{i-T} = 8.7 × 10^{-6} Å^{-2} with the incubation time. It is worth noting that, at 24 h incubation, the ρ_{i-T} value was close to the theoretically calculated ρ of hydrocarbon chains of POPC/POPE (ρ = 7.8 × 10^{-6} Å^{-2}), indicating a fully formed mature bilayer. Moreover, the inner hydrocarbon tail thickness, $t_{i\text{-T}}$, increased from 11.4 Å at 3 h to 17.3 Å at 24 h, while the outer leaflet hydrocarbon tail thickness was constant at $t_{o\text{-T}}$ ~ 15.7 Å.

Based on these results, *i.e.* a significant increase in both $t_{i\text{-T}}$ and ρ_{o-T}, as well as a decrease in ρ_{i-T}, we propose that structural rearrangement occurred with the incubation time, with the QDs progressively expelled from the inner leaflet to the outer leaflet of the bilayer. The schematic of this proposed structural evolution and QD rearrangement is shown in **Figure 3 (C)**. Our previous QCM-D study showed that the incorporation of the hydrophobic QDs encouraged the vesicle to rupture, with fusion occurring at a lower critical surface liposomal coverage compared to liposomes without QDs.[18] QDs embedded in the hydrophobic region of the bilayer can have a direct effect on the conformation of the hydrocarbon chains, and thus the membrane elastic properties. These interactions can induce a substantial structural reorganization in the POPC/POPE bilayer adjacent to the QDs due to the reorientation of the lipid molecules. As a result, the QD-endowed liposomes undergo rupture to form lipid bilayers with conformationally disordered alkyl chains, which are likely tilted or coiled due to the presence of the hydrophobic QDs. Our XRR data suggests that this initial bilayer formation is followed by progressive QD rearrangement from the inner leaflet (*i.e.* proximal to the substrate) towards the outer leaflet (*i.e.* distal to the substrate), indicated by more ordered lipid chains in the inner leaflet of POPC/POPE bilayer due to enhanced lipid packing that further decreased the conformational entropy of the system. Meanwhile, the outer leaflet in contact with water is less constrained, and thus more readily deformed to accommodate the QDs. This mechanism for the temporal structural evolution of QD-SLBs *via* the liposome fusion route has not been previously reported.

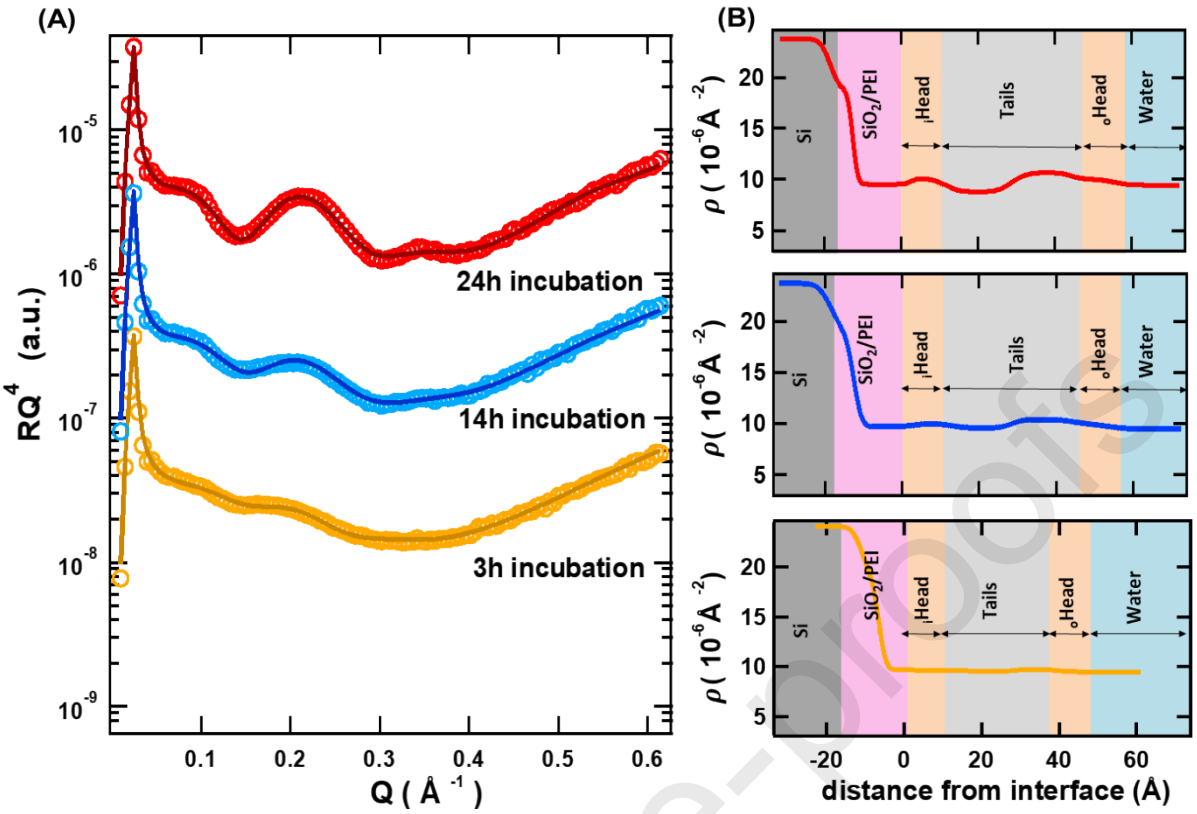

Figure 4. X-ray reflectivity curves of POPC/POPE lipid bilayers with 4.9 nm CdS QDs (QD-SLBs) at 3 h, 14 h, and 24 h incubation time (A) and corresponding SLD profiles with different coloured regions highlighting different layers across the interface (B).

Complementary AFM imaging was also performed to observe the QD-SLB topography of the bilayers as a function of the incubation time (**Figure 5**), showing changes over the incubation time. The morphology of pure SLBs is included in the **SM**. In the case of the QD-SLBs, at 3 h (**Figure 5 (A)**), the surface coverage of the bilayer (*i.e.* lighter coloured regions) was low, with some unruptured liposomes or their aggregates also observed atop the bilayer/substrate, as the corresponding line profiles suggest. The surface bilayer coverage increased over the incubation time, with more surface areas covered by SLBs at 14 h and 24 h incubation time. We note that the line profiles showed smaller bilayer thickness compared to the XRR data, which could be attributed to the soft and thus not-so-well defined PEI polymer cushion underlayer; it would make it difficult to ascertain the thickness of the bilayer atop. Such AFM imaging revealed the local topography over a relatively small area (4 µm×2 µm), whereas XRR measurement averaged over a much larger footprint (1 mm×100 µm) and thus is more representative of the average thickness over the whole sample area.

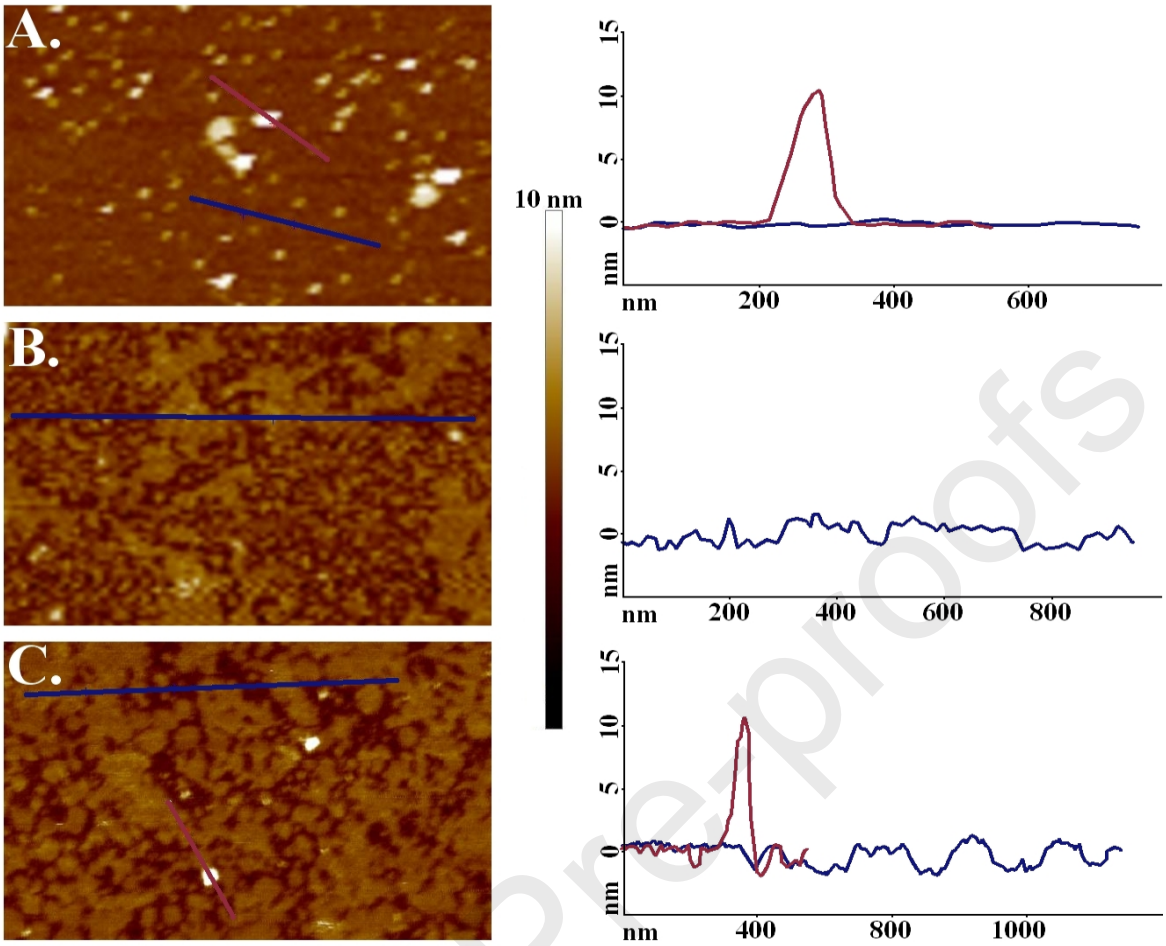

Figure 5. AFM images and line profiles deposited POPC/POPE SUVs with QDs after incubation time of 3 h (A), 14 (B) and 24 h (C). All the height scale bars in the Figure represent 10 nm.

CONCLUSIONS

In this study, the temporal structural evolution of supported POPC/POPE lipid bilayers intercalated with hydrophobic QDs (QD-SLBs) on a PEI polymer cushion has been reported. The supported bilayers were formed *via* fusion of QD-embedded liposomes on the substrate. Synchrotron XRR has been applied to investigate structural characteristics of the lipid bilayers, including thickness, interfacial roughness, and surface coverage. The high flux of the synchrotron X-rays facilitated relatively high temporal resolution to track the bilayer structural evolution over a period of 24 h after initial SLB formation. The initial thickness of the QD-SLBs was smaller (t = 44.2 Å) compared to the SLBs without QDs (t = 48.3 Å). The structure of the QD-SLBs evolved with the incubation time. Bilayers became thicker (t = 49.1 Å at 14 h incubation and t = 52.9 Å at 24 h incubation). This was attributed to the rearrangement of CdS QDs and lipids in the bilayer with the increasing incubation time. The fitted scattering length density (SLD) profiles suggest that the QDs were expelled from the inner leaflet to the outer leaflet of the bilayer. Such structural reorganisation was related to the insertion of hydrophobic

QDs in the hydrocarbon tails region of the SLBs, which enhanced disorder in the conformation of the lipid chains in the POPC/POPE bilayer. Initially (at 3 h incubation), this reduced membrane thickness was due to lipid tails tilting to accommodate the hydrophobic QDs. Subsequent QD expulsion from the inner membrane led to a more ordered packing of the lipid molecules in the inner leaflet, whilst the outer membrane leaflet in contact with water, less constrained and more flexible, more readily accommodated the QDs. This led to the observed changes in the thicknesses of the inner and outer membranes with the incubation time. These unprecedented results provide valuable structural information on the structure of QD-containing fluorescent SLBs, giving mechanistic insights on the QD-SLB formation process, kinetics, and structural evolution, with implications for biosensing, drug delivery and nanoparticle cytotoxicity, in which the interactions between nanoparticles and membranes are an important consideration. It will be useful and interesting, using XRR and NR methods, to further examine in detail structural evolution of QD/nanoparticle containing SLBs, investigating the effects of the QD surface chemistry and size, temperature, SLB lipid composition, and different types of the polyelectrolyte cushion. In particular, the contrast match capacity of NR could offer information on the distributions of different constituents in the QD-endowed SLBs. This remains a focus of our future studies.

Acknowledgements

This research was funded in part by the National Science Centre, Poland, Contract No. UMO-2016/23/B/ST8/03128 and the statutory research fund of ICSC PAS. The XRR was performed at the ESRF BM28 (XMaS) beamline, which is a mid-range facility supported by EPSRC. We are grateful to all the beamline team staff for their support. The European Union Erasmus+ programme (project number: 2016-1-PL01-KA103-023786) is acknowledged for providing scholarship (financial support) for the research/mobility/traineeship. Funding from the Engineering and Physical Science Research Council (EPSRC EP/L016648/1; L.J.F.), Procter & Gamble (A.S.), and Infinuem and the Everett Bequest Fund (N.T.) is gratefully acknowledged.

REFERENCES

[1] J. Salafsky, J.T. Groves, S.G. Boxer, Architecture and function of membrane proteins in planar supported bilayers: A study with photosynthetic reaction centers, Biochemistry. 35 (1996) 14773–14781.

[2] L.A. Kung, L. Kam, J.S. Hovis, S.G. Boxer, Patterning hybrid surfaces of proteins and supported lipid bilayers, Langmuir. 16 (2000) 6773–6776.

[3] S. Boudard, B. Seantier, C. Breffa, G. Decher, O. Félix, Controlling the pathway of formation of supported lipid bilayers of DMPC by varying the sodium chloride concentration, Thin Solid Films. 495 (2006) 246–

251.
[4] R. Tero, Substrate effects on the formation process, structure and physicochemical properties of supported lipid bilayers, Materials (Basel). 5 (2012) 2658–2680.
[5] K. Mulligan, Z.J. Jakubek, L.J. Johnston, Supported lipid bilayers on biocompatible polysaccharide multilayers, Langmuir. 27 (2011) 14352–14359.
[6] E. Kalb, S. Frey, L.K. Tamm, Formation of supported planar bilayers by fusion of vesicles to supported phospholipid monolayers, BBA - Biomembr. 1103 (1992) 307–316.
[7] A. Oshima, K. Sumitomo, Vesicle fusion with bilayer lipid membrane controlled by electrostatic interaction, Biochem. Biophys. Reports. 11 (2017) 58–63.
[8] T.K. Lind, M. Cárdenas, H.P. Wacklin, Formation of supported lipid bilayers by vesicle fusion: Effect of deposition temperature, Langmuir. 30 (2014) 7259–7263.
[9] C.J. Brinker, Y. Lu, A. Sellinger, H. Fan, Evaporation-induced self-assembly: Nanostructures made easy, Adv. Mater. 11 (1999) 579–585.
[10] U. Mennicke, T. Salditt, Preparation of solid-supported lipid bilayers by spin-coating, Langmuir. 18 (2002) 8172–8177.
[11] F. Tiberg, I. Harwigsson, M. Malmsten, Formation of model lipid bilayers at the silica-water interface by co-adsorption with non-ionic dodecyl maltoside surfactant, Eur. Biophys. J. 29 (2000) 196–203.
[12] J. Liu, J.C. Conboy, Structure of a gel phase lipid bilayer prepared by the Langmuir-Blodgett/ Langmuir-Schaefer method characterized by sum-frequency vibrational spectroscopy, Langmuir. 21 (2005) 9091–9097.
[13] T. Baumgart, A. Offenhäuser, Polysaccharide-supported planar bilayer lipid model membranes, Langmuir. 19 (2003) 1730–1737.
[14] M. Ross, C. Steinem, H.J. Galla, A. Janshoff, Visualization of chemical and physical properties of calcium-induced domains in DPPC/DPPS Langmuir-Blodgett layers, Langmuir. 17 (2001) 2437–2445.
[15] A.A. Brian, H.M. McConnell, Allogeneic stimulation of cytotoxic T cells by supported planar membranes, Proc. Natl. Acad. Sci. U. S. A. 81 (1984) 6159–6163.
[16] D. Levy, P.E. Milhiet, Imaging of transmembrane proteins directly incorporated within supported lipid bilayers using atomic force microscopy, Methods Mol. Biol. 950 (2013) 343–357.
[17] N. Sakaguchi, Y. Kimura, A. Hirano-Iwata, T. Ogino, Fabrication of Au-Nanoparticle-Embedded Lipid Bilayer Membranes Supported on Solid Substrates, J. Phys. Chem. B. 121 (2017) 4474–4481.
[18] M. Wlodek, M. Kolasinska-Sojka, M. Szuwarzynski, S. Kereïche, L. Kovacik, L. Zhou, L. Islas, P. Warszynski, W.H. Briscoe, Supported lipid bilayers with encapsulated quantum dots (QDs): Via liposome fusion: Effect of QD size on bilayer formation and structure, Nanoscale. 10 (2018) 17965–17974.
[19] M. Kolasinska-Sojka, M. Wlodek, M. Szuwarzynski, S. Kereiche, L. Kovacik, P. Warszynski, Properties of POPC/POPE supported lipid bilayers modified with hydrophobic quantum dots on polyelectrolyte cushions, Colloids Surfaces B Biointerfaces. 158 (2017) 667–674.
[20] G.J. Hardy, R. Nayak, S. Zauscher, Model cell membranes: Techniques to form complex biomimetic supported lipid bilayers via vesicle fusion, Curr. Opin. Colloid Interface Sci. 18 (2013) 448–458.
[21] E. Reimhult, F. Höök, B. Kasemo, Vesicle adsorption on SiO2 and TiO2: Dependence on vesicle size, J. Chem. Phys. 117 (2002) 7401–7404.
[22] B. Scantier, C. Breffa, O. Félix, G. Decher, Dissipation-enhanced quartz crystal microbalance studies on the experimental parameters controlling the formation of supported lipid bilayers, J. Phys. Chem. B. 109 (2005) 21755–21765.
[23] E. Reimhult, F. Hook, B. Kasemo, Temperature dependence of formation of a supported phospholipid bilayer from vesicles on SiO2, Phys. Rev. 66 (2002).
[24] B. Seantier, B. Kasemo, Influence of mono- and divalent ions on the formation of supported phospholipid bilayers via vesicle adsorption, Langmuir. 25 (2009) 5767–5772.
[25] D. Meléndrez, T. Jowitt, M. Iliut, A.F. Verre, S. Goodwin, A. Vijayaraghavan, Adsorption and binding dynamics of graphene-supported phospholipid membranes using the QCM-D technique, Nanoscale. 10 (2018) 2555–2567.
[26] M. Wlodek, M. Kolasinska-Sojka, M. Wasilewska, O. Bikondoa, W.H. Briscoe, P. Warszynski, Interfacial and structural characteristics of polyelectrolyte multilayers used as cushions for supported lipid bilayers, Soft Matter. 13 (2017) 7848–7855.
[27] M. Wlodek, M. Szuwarzynski, M. Kolasinska-Sojka, Effect of Supporting Polyelectrolyte Multilayers and Deposition Conditions on the Formation of 1-Palmitoyl-2-oleoyl-sn-glycero-3-phosphocholine/1-Palmitoyl-2-oleoyl-sn-glycero-3-phosphoethanolamine Lipid Bilayers, Langmuir. 31 (2015) 10484–10492.
[28] E. Reimhult, B. Kasemo, F. Höök, Rupture pathway of phosphatidylcholine liposomes on silicon dioxide, Int. J. Mol. Sci. 10 (2009) 1683–1696.
[29] M. Costanzo, F. Carton, A. Marengo, G. Berlier, B. Stella, S. Arpicco, M. Malatesta, Fluorescence and

electron microscopy to visualize the intracellular fate of nanoparticles for drug delivery, Eur. J. Histochem. 60 (2016) 2640.
[30] J. Yang, A. Bahreman, G. Daudey, J. Bussmann, R.C.L. Olsthoorn, A. Kros, Drug delivery via cell membrane fusion using lipopeptide modified liposomes, ACS Cent. Sci. 2 (2016) 621–630.
[31] I. Bruzas, S. Unser, S. Yazdi, E. Ringe, L. Sagle, Ultrasensitive plasmonic platform for label-free detection of membrane-associated species, Anal. Chem. 88 (2016) 7968–7974.
[32] C. Montis, D. Maiolo, I. Alessandri, P. Bergese, D. Berti, Interaction of nanoparticles with lipid membranes: A multiscale perspective, Nanoscale. 6 (2014) 6452–6457.
[33] C.M. Beddoes, C.P. Case, W.H. Briscoe, Understanding nanoparticle cellular entry: A physicochemical perspective, Adv. Colloid Interface Sci. 218 (2015) 48–68.
[34] N. Biswas, R. Bhattacharya, A. Saha, N.R. Jana, J.K. Basu, Interplay of electrostatics and lipid packing determines the binding of charged polymer coated nanoparticles to model membranes, Phys. Chem. Chem. Phys. 17 (2015) 24238–24247.
[35] A.C. Mensch, J.T. Buchman, C.L. Haynes, J.A. Pedersen, R.J. Hamers, Quaternary Amine-Terminated Quantum Dots Induce Structural Changes to Supported Lipid Bilayers, Langmuir. 34 (2018) 12369–12378.
[36] R. Michel, M. Gradzielski, Experimental Aspects of Colloidal Interactions in Mixed systems of liposome and inorganic nanoparticle and their applications, Int. J. Mol. Sci. 13 (2012) 11610–11642.
[37] C. Montis, V. Generini, G. Boccalini, P. Bergese, D. Bani, D. Berti, Model lipid bilayers mimic non-specific interactions of gold nanoparticles with macrophage plasma membranes, J. Colloid Interface Sci. 516 (2018) 284–294.
[38] M. Mendozza, L. Caselli, C. Montis, S. Orazzini, E. Carretti, P. Baglioni, D. Berti, Inorganic nanoparticles modify the phase behavior and viscoelastic properties of non-lamellar lipid mesophases, J. Colloid Interface Sci. 541 (2019) 329–338.
[39] K. Murzyn, T. Rog, M. Pasenkiewicz-Gierula, Phosphatidylethanolamine-phosphatidylglycerol bilayer as a model of the inner bacterial membrane, Biophys. J. 88 (2005) 1091–1103.
[40] N. Kučerka, F.A. Heberle, J. Pan, J. Katsaras, Structural significance of lipid diversity as studied by small angle neutron and X-ray scattering, Membranes (Basel). 5 (2015) 454–472.
[41] D. a Pink, S. McNeil, B. Quinn, M.J. Zuckermann, A model of hydrogen bond formation in phosphatidylethanolamine bilayers., Biochim. Biophys. Acta. 1368 (1998) 289–305.
[42] M. Kolasinska, R. Krastev, P. Warszynski, Characteristics of polyelectrolyte multilayers: Effect of PEI anchoring layer and posttreatment after deposition, J. Colloid Interface Sci. 305 (2007) 46–56.
[43] M. Wlodek, M. Kolasinska-Sojka, M. Szuwarzynski, S. Zapotoczny, P. Warszynski, Formation and characterization of (1-palmitoyl-2-oleoyl-sn-glycero-3-phosphocholine)/(1-palmitoyl-2-oleoyl-sn-glycero-3-phospho-l-serine) supported lipid bilayers on polyelectrolyte multilayer films, Thin Solid Films. 592 (2015) 1–7.
[44] Z. Adamczyk, A. Michna, M. Szaraniec, A. Bratek, J. Barbasz, Characterization of poly(ethylene imine) layers on mica by the streaming potential and particle deposition methods, J. Colloid Interface Sci. 313 (2007) 86–96.
[45] W.H. Briscoe, F. Speranza, P. Li, O. Konovalov, L. Bouchenoire, J. van Stam, J. Klein, R.M.J. Jacobs, R.K. Thomas, Synchrotron XRR study of soft nanofilms at the mica–water interface, Soft Matter. 8 (2012) 5055–5068.
[46] A. Nelson, Co-refinement of multiple-contrast neutron/X-ray reflectivity data using MOTOFIT, J. Appl. Crystallogr. 39 (2006) 273–276.
[47] Z. V. Leonenko, E. Finot, H. Ma, T.E.S. Dahms, D.T. Cramb, Investigation of temperature-induced phase transitions in DOPC and DPPC phospholipid bilayers using temperature-controlled scanning force microscopy, Biophys. J. 86 (2004) 3783–3793.
[48] M. Pasenkiewicz-Gierula, K. Murzyn, T. Róg, C. Czaplewski, Molecular dynamics simulation studies of lipid bilayer systems, Acta Biochim. Pol. (2000) 601–611.
[49] M. Vogel, C. Münster, W. Fenzl, T. Salditt, Thermal unbinding of highly oriented phospholipid membranes, Phys. Rev. Lett. 84 (2000) 390–393.
[50] M. Golub, D. Lott, E.B. Watkins, V. Garamus, B. Luthringer, M. Stoermer, A. Schreyer, R. Willumeit, X-ray and neutron investigation of self-assembled lipid layers on a titanium surface, Biointerphases. 8 (2013) 1–11.
[51] J.M. Boggs, Lipid intermolecular hydrogen bonding: influence on structural organization and membrane function, BBA - Rev. Biomembr. (1987) 353–404.
[52] A.M. Sendecki, M.F. Poyton, A.J. Baxter, T. Yang, P.S. Cremer, Supported Lipid Bilayers with Phosphatidylethanolamine as the Major Component, Langmuir. 33 (2017) 13423–13429.
[53] A.A. Gurtovenko, I. Vattulainen, Lipid transmembrane asymmetry and intrinsic membrane potential: Two sides of the same coin, J. Am. Chem. Soc. 129 (2007) 5358–5359.

[54] B. Eicher, D. Marquardt, F.A. Heberle, I. Letofsky-Papst, G.N. Rechberger, M.S. Appavou, J. Katsaras, G. Pabst, Intrinsic Curvature-Mediated Transbilayer Coupling in Asymmetric Lipid Vesicles, Biophys. J. 114 (2018) 146–157.

[55] S. May, Y. Kozlovsky, A. Ben-Shaul, M.M. Kozlov, Tilt modulus of a lipid monolayer, Eur. Phys. J. E. 14 (2004) 299–308.

[56] A. Gupta, H. Saxena, R.P. Giri, G. Bhattacharya, M.K. Mukhopadhyay, S.K. Ghosh, V. V. Agrawal, X-ray Reflectivity Study of the Interaction of an Imidazolium-Based Ionic Liquid with a Soft Supported Lipid Membrane, Langmuir. 33 (2017) 1295–1304.

[57] L. Zhou, L. Islas, N. Taylor, O. Bikondoa, E. Robles, W.H. Briscoe, Graphene surface structure in aqueous media: Evidence for an air-bubble layer and ion adsorption, Carbon N. Y. 143 (2019) 97–105.

[58] K. Lai, B. Wang, Y. Zhang, Y. Zheng, Computer simulation study of nanoparticle interaction with a lipid membrane under mechanical stress, Phys. Chem. Chem. Phys. 15 (2013) 270–278.

[59] P. Gkeka, P. Angelikopoulos, L. Sarkisov, Z. Cournia, Membrane Partitioning of Anionic, Ligand-Coated Nanoparticles Is Accompanied by Ligand Snorkeling, Local Disordering, and Cholesterol Depletion, PLoS Comput. Biol. 10 (2014) e1003917.

[60] P.R. Leroueil, S.A. Berry, K. Duthie, G. Han, V.M. Rotello, D.Q. McNerny, J.R. Baker, B.G. Orr, M.M.B. Holl, Wide varieties of cationic nanoparticles induce defects in supported lipid bilayers, Nano Lett. 8 (2008) 420–424.

Declaration of interests

☒ The authors declare that they have no known competing financial interests or personal relationships that could have appeared to influence the work reported in this paper.

☐The authors declare the following financial interests/personal relationships which may be considered as potential competing interests: